EUROPEAN ORGANIZATION FOR NUCLEAR RESEARCH
European Laboratory for Particle Physics

Publication
ALICE reference number
ALICE-PUB-2001-57 version 1.0
Institute reference number

Date of last change
2001-12-13

Heavy quarks with ALICE

Authors:

P. Crochet
for the ALICE collaboration

EPJdirect A1, 1–11 (2001)
DOI 10.1007/s1010501a123

EPJdirect
electronic only

Heavy quark measurements with ALICE

P. Crochet for the ALICE collaboration

Laboratoire de Physique Corpusculaire
IN2P3/CNRS and Université Blaise Pascal
F-63000 Clermont-Ferrand, France
e-mail: crochet@clermont.in2p3.fr

Received:

Abstract. The capabilities of ALICE to measure hidden and open heavy flavours in nucleus-nucleus collisions at the LHC are reviewed.

PACS: 25.75.-q; 24.85.+p

1 Introduction

The LHC heavy ion physics program aims at investigating the properties of strongly interacting matter at extreme energy density where the formation of the Quark Gluon Plasma (QGP) is expected [1]. Among the most promising observables, heavy quarkonium states are especially relevant since they provide, via their leptonic decays, an essential probe of the earliest and hottest stages of heavy ion collisions. From the early predictions of charmonium suppression by Debye screening in a deconfined medium [2] to the recent results from the NA50 collaboration [3], a lot of effort has been devoted to the subject (for reviews see [4, 5]). The LHC energy is ideal for a spectroscopy of the whole set of resonances. In particular, because a much higher temperature than that expected to be reached at RHIC is needed to dissolve the Υ meson, the spectroscopy of the Υ family at LHC energies should reveal an unique set of information on the characteristics of the QGP [6]. On the other hand, the study of heavy quark resonances at the LHC is subject to significant differences with respect to the SPS energies. First of all the signals will be sitting on top of a complex combinatorial background, mainly coming from open charm and open bottom decay [7]. Then, in addition to prompt charmonia produced "directly" via hard scattering, secondary charmonia can be produced from bottom decay [8], $D\bar{D}$ annihilation [9, 10] and statistical hadronization [11, 12, 13]. Furthermore, the SPS results have demonstrated that the study of onium suppression must be closely joined to the study of open heavy flavours because both open and hidden quarkonia arise from the same underlying production mechanism. Although it is commonly admitted that, at the LHC, a large production rate of $c\bar{c}$ and $b\bar{b}$ pairs is expected[1], the present estimations for heavy flavour production in nucleon-nucleon collisions are subject to some

[1] Up to 115 $c\bar{c}$ and 5 $b\bar{b}$ should to be produced per central (5% of the total cross-section) PbPb collision [14].

uncertainties [14]. In addition, in the environment of an heavy ion reaction, energy loss of heavy quarks might substantially modify the spectra of the decay particles (see [15] and references therein).

It is therefore obvious that a meaningful understanding of the QGP requires to perform systematic investigations. Indeed, the signals have to be measured:

- as a function of centrality (to find threshold-like behaviour(s) à la NA50)
- as a function of system-size (to disentangle normal and abnormal suppression)
- for all onium species (because individual survival probabilities probe Debye screening)
- as a function of p_{t} (to disentangle QGP models)
- together with open charm and open bottom (which is the most natural normalization of the quarkonium signals)
- with good vertex resolution (to disentangle prompt and secondary charmonia)
- versus the reaction plane (to unravel Glauber and comover absorption)
- together with other QGP signals

This physics program should be achievable with the ALICE detector [16]. Quarkonium states will be identified in the dielectron and the dimuon channels. Open charm and bottom will be measured in the hadronic and the semi-leptonic decay channels of heavy mesons. The expected performances in these different channels are presented in the following. For further details about hadronic measurements and proton-proton physics with ALICE, see [17] and [18], respectively.

2 Dimuon

The ALICE forward muon spectrometer covers the angular acceptance $2^\circ < \Theta < 9^\circ$ ($2.5 < \eta < 4$). It makes use of the usual techniques for muon identification at small angles. The spectrometer consists of a front absorber placed 90 cm from the interaction point, a 15 m long small angle absorber, a large dipole magnet with a 3 Tm integrated field, 10 high granularity tracking chambers, a muon filter made of a 1.2 m thick iron wall and 4 large area trigger chambers [19, 20, 21, 22]. The goal of the forward muon spectrometer is to measure the full set of onium resonances from the ϕ to the Υ, with a high statistics, a low background and a high resolution (Fig. 1).

An important specification of the spectrometer is its mass resolution which has to be about 100 MeV at 10 GeV to allow the separation of the Υ substates. Therefore a lot of simulations has been done in order to understand the mass resolution and to keep it as good as possible. These simulations have been performed in the framework of the ALICE software AliRoot [24]. They consist of i) transport of particles through the apparatus, ii) digitalization of the detector

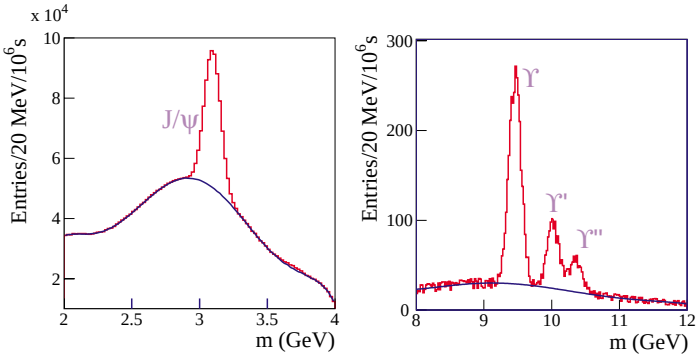

Fig. 1. Unlike-sign dimuon mass spectra in the region $2 < m < 4$ GeV (left) and $8 < m < 12$ GeV (right) for the 10% most-central PbPb reactions. The spectra were obtained by means of fast simulations including acceptance cuts and detector efficiencies and resolutions. They correspond to a luminosity of $5 \cdot 10^{26}$ cm^{-2}s^{-1} and a running time of 10^6 s. From [20, 23].

response, iii) reconstruction of raw clusters, and iv) tracking of the reconstructed points. A very detailed description of all the relevant detector components is included. In particular, as far as the front and small angle absorbers are concerned, the flanges, dips, recesses and spaces as well as the different materials were taken into account [22]. The input to the simulation consists of one Υ embedded into one central PbPb event. The latter is generated according to the HIJING model which foresees the largest charged particle multiplicity ($[\mathrm{dN_{ch}}/\mathrm{d}\eta]_{\eta=0} = 6000$). In addition a safety factor of two is applied such that one nominal background event (or "background level 1") actually consists of two times one HIJING central PbPb event.

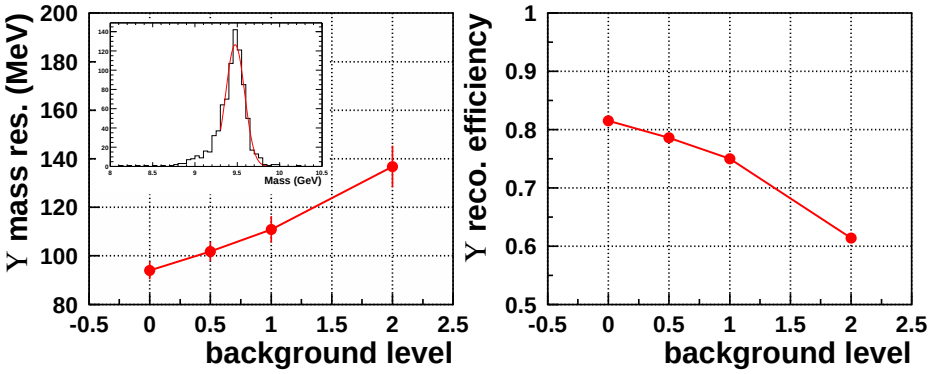

Fig. 2. Left: Υ mass resolution, from one single Gaussian fit to the mass distribution between 9.30 and 9.85 GeV, as a function of the background level with respect to the nominal background. The inset shows the corresponding mass distribution for background level 1. Right: Υ reconstruction efficiency as a function of the background level with respect to the nominal background.

The corresponding Υ mass resolution is shown in Fig. 2 left as a function of the background level. The obtained resolution without any background (background level 0) of $\sim$ 92 MeV is larger than the intrinsic mass resolution of the spectrometer by about 10 MeV. This is the result of muon energy losses which spread the mass distribution on the left side of the Υ nominal mass (inset in Fig. 2 left). With background level 1 the mass resolution increases up to 110 MeV. This value is extracted from a single Gaussian fit to the mass distribution. When performing a two Gaussian fit to account for the particular shape of the mass distribution, the corresponding resolution is 94.5 MeV. Such a resolution should allow to unfold the contribution from Υ' and Υ'' resonances.

The Υ reconstruction efficiency is shown in Fig. 2 right as a function of the background level. For background level 1 the total Υ reconstruction efficiency is 75%. This value corresponds to the convolution of the following efficiencies:

geometrical acceptance ..... $\sim 95\%$
chamber intrinsic efficiency & resolution ..... $\sim 96\%$
tracking ..... $\sim 95\%$
tails in mass distribution (3σ mass cut) ..... $\sim 93\%$
multi-hit deconvolution ..... $\sim 92.5\%$

The efficiency increases towards 80% for lower background level. The trigger efficiency for Υ is 90% [21].

The acceptance versus $p_{\rm t}$ for ϕ, J/ψ and Υ is shown in Fig. 3. The ϕ acceptance is limited at low $p_{\rm t}$ owing to the momentum cut of about 4 GeV/c introduced by energy loss in the absorbers. The acceptance for J/ψ and Υ is fairly uniform in $p_{\rm t}$, down to $p_{\rm t} = 0$. It reaches a maximum of 45% and 60%, respectively, around rapidity 3.3 [20].

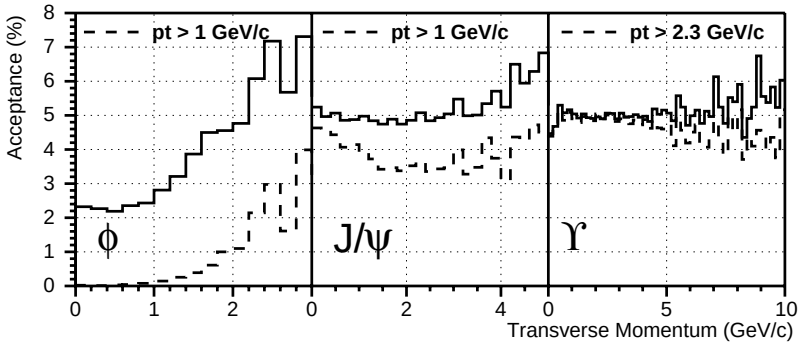

Fig. 3. Acceptance as a function of transverse momentum for ϕ, J/ψ and Υ without (solid histograms) and with (dashed histograms) the trigger cut on single muon $p_{\rm t}$ indicated on the figures.

The expected statistics after one month of Pb beams is shown in Tab. 1. For J/ψ, the rate and S/B are very good and permit a high-precision measurement of its production as a function of $p_{\rm t}$. Because of less favourable S/B, the ψ' can be measured at best with an accuracy of the order of 10%. The S/B is far better

in the Υ mass range. It is larger than unity in all cases and the significance is very good. Note however that the rates are small, especially for the Υ''.

	S	S/B	$S/\sqrt{S+B}$
J/ψ	230000	0.72	310
ψ'	4600	0.03	12
Υ	1800	7.10	39
Υ'	540	2.50	19
Υ''	260	1.50	12

Table 1. Expected signal, signal-to-background and significance for different onium states in 10% most-central PbPb reactions with a luminosity of $5 \cdot 10^{26}$ cm^{-2}s^{-1} and a running time of 10^6 s. Detector efficiencies and analysis cuts are taken into account. The production cross-sections folded with the muonic branching ratio per side ($y > 0$) are 14.3 mb and 130 μb for J/ψ and Υ, respectively. The relative production cross-section times branching ratios of the higher Υ states are assumed to be $\sigma\mathrm{Br}(\Upsilon) : \sigma\mathrm{Br}(\Upsilon') : \sigma\mathrm{Br}(\Upsilon'') = 1 : 0.3 : 0.15$. The production cross-section of ψ' is assumed to be a factor 5 lower than that of J/ψ. S and B are extracted according to the interval of $\pm 1\sigma$ around the resonance nominal mass. See [20] for more details.

In addition to quarkonia measurements, the muon spectrometer should allow measurements of the open bottom cross-section. This is possible because the background from pions and kaons decay is small and because muons from charm decay can be efficiently removed with a high p_t threshold. As illustrated in Fig. 4, when applying a p_t cut of 3 GeV/c on each muon, the correlated signal from bottom decay appears with a large relative yield all over the invariant mass.

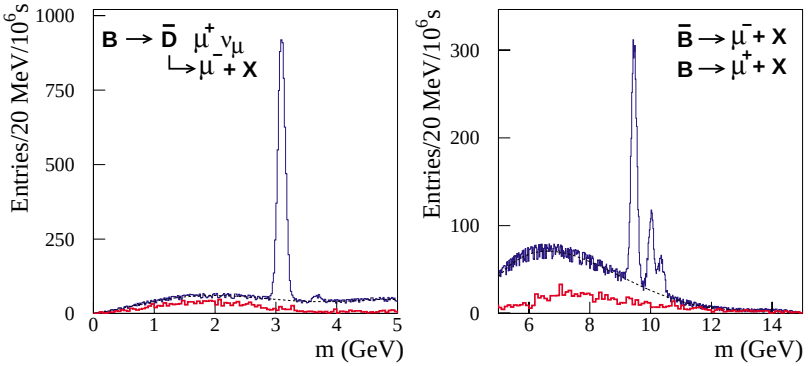

Fig. 4. Unlike-sign dimuon mass spectra in the region $0 < m < 5$ GeV (left) and $5 < m < 15$ GeV (right) for central PbPb reactions. A p_t threshold of 3 GeV/c is applied on each single muon. The upper and lower histogram correspond to the total combinatorial background and to the correlated signal from bottom decay, respectively. The spectra were obtained by means of fast simulations. From [25].

This should allow to extract the full correlated signal from bottom decay including both the high and the low invariant mass regions. In the high invariant mass region (Fig. 4 right) each muon comes from the direct decay of a B meson. In the low invariant mass region (Fig. 4 left), the correlated signal from bottom is dominated by the so-called B-chain channel where the two muons come from the decay of a single B meson via a D meson. Similar measurements of the charm cross-section should be achievable with appropriate analysis strategies.

3 Dielectron

The measurement of dielectron in the central barrel of ALICE is complementary to the above discussed dimuon channel. Firstly, this extends quarkonia measurements from the forward rapidity region to mid-rapidity. Then, the vertex capabilities of the ITS allow to measure secondary J/ψ from bottom decay. This will not only permit distinction between primary and secondary J/ψ, but also lead to a direct measurement of the B meson production cross-section. Furthermore, single high p_{t} electrons with displaced vertex give access to the inclusive open charm and open bottom cross-sections. This measurement is complementary to the measurement of open heavy flavours from the dilepton continuum, as discussed in the previous section, and to the reconstruction of heavy mesons in the hadronic channel (see next section). It brings essential information, in particular, in order to normalize the quarkonia signals as discussed in the introduction.

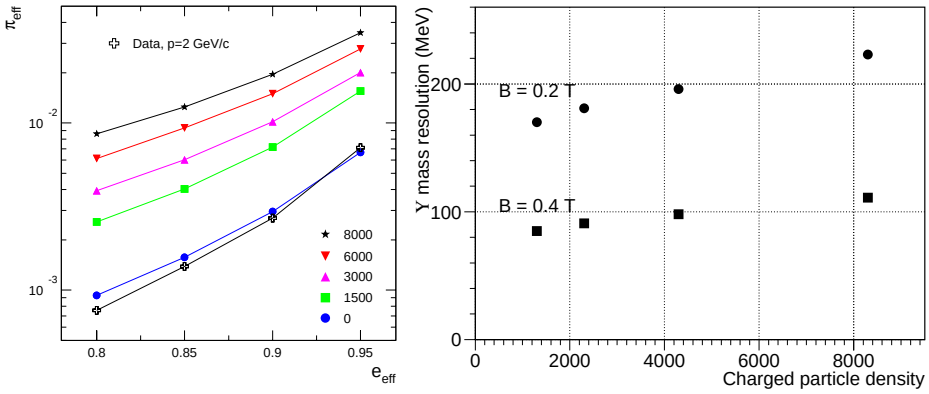

Fig. 5. Left: pion efficiency as a function of electron efficiency for different charged particle densities at mid-rapidity and tracks of $p = 2$ GeV/c total momentum. Right: invariant mass resolution for Υ decaying into $\mathrm{e}^{+}\mathrm{e}^{-}$ as a function of the charged particle density at mid-rapidity when both tracks are reconstructed in the TPC and the ITS. The resolution is shown for two different settings of the magnetic field.

The centerpiece for dielectron physics is the TRD (Transition Radiation Detector) which provides an electron trigger and identification [26, 27]. Its expected pion rejection factor is of the order of 100 for 90% electron identification efficiency and tracks with $p > 1$ GeV/c. Its acceptance is identical to that of the

ITS/TPC ($|\eta| < 0.9$ with full azimuthal coverage[2]). It is made of 540 modules ($18(\phi) \times 5(\mathrm{Z}) \times 6(\mathrm{layers})$). Each module consists of a radiator where the transition radiation is produced and a readout chamber where the transition radiation is measured along with the ionization energy loss. The total number of channels and active surface are $1.2 \cdot 10^6$ and 740 m^2, respectively.

The performances of the TRD in a high multiplicity environment have been investigated with the previously mentioned AliRoot software. The multiplicity dependence of the pion rejection factor for different electron identification efficiencies is shown in the left panel of Fig. 5. The simulations were adjusted to test beam data [28] for well isolated tracks (dots in Fig. 5 left) and then performed for various track multiplicities. Going from well isolated tracks to a full multiplicity event (8000 charged particles per unit of rapidity at mid-rapidity), a worsening of the pion rejection factor by a factor 6-7 is observed. For an electron efficiency of 90% the pion rejection factor is still better than 50. A further improvement of 30-40% can be achieved [27].

The best momentum resolution for electrons identified with the TRD will be obtained by combining the information of the TRD, TPC and ITS in a global fit. Such a procedure is currently being optimized. Using the track reconstruction in the TPC and ITS, but yet without the TRD, the Υ mass resolution shown in the right panel of Fig. 5 is obtained. It can be seen that, even for the highest anticipated charged particle density, the Υ mass resolution is of the order of 100 MeV, thus allowing a separation of the Υ substates, provided that one uses a magnetic field of at least 0.4 T.

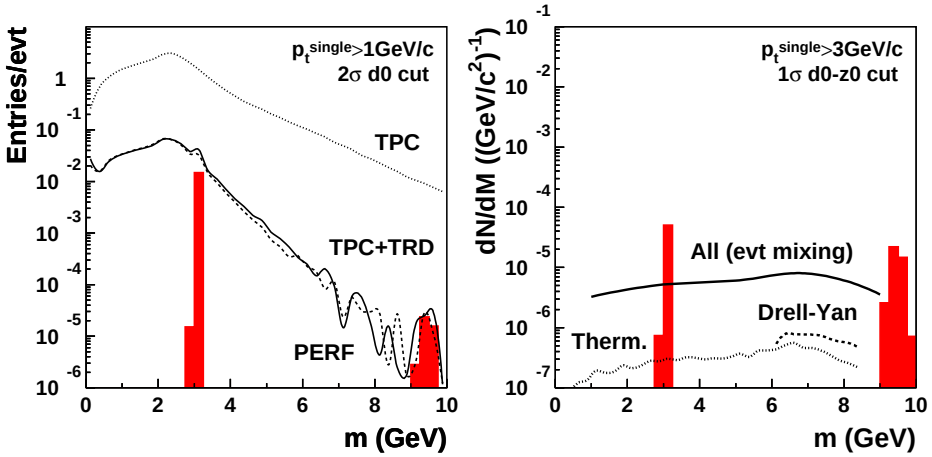

Fig. 6. Left: invariant mass spectrum of dielectron with a transverse momentum cut of 1 GeV/c on electron candidates. The shaded areas show the signal for J/ψ and Υ. The spectra were obtained by means of fast simulations including geometrical acceptance cuts, detector efficiencies and resolutions and assuming a magnetic field of 0.2 T. Right: same with a transverse momentum cut of 3 GeV/c.

The physics perspectives opened with the TRD have been investigated by

[2]Only half of the TRD accceptance is currently financed [16].

means of fast simulations. Figure 6 left shows once more the excellent capability of the TRD for electron identification. The dotted histogram corresponds to the dielectron invariant mass distribution obtained with only the ITS/TPC. The corresponding electron sample is contaminated to a large extent by mis-identified pions[3]. As shown by the dashed histogram, the TRD allows to get rid of most of these mis-identified pions. The final spectrum is similar to that which would be obtained with a perfect particle identification (solid histogram) thus allowing a precise determination of the resonance yields.

On the other hand, once the average number of electron per event is substantially below one, the combinatorial background should be strongly reduced. As an example the right panel of Fig. 6 displays the situation with a p_t cut of 3 GeV/c on each electron (the thermal radiation curve is from [29]). This permits to access the continuum in the invariant mass spectrum between J/ψ and Υ which carries contributions from thermal plasma radiation and direct production (Drell-Yan). According to Fig. 6, a signal-to-background of 1:10 is expected.

The very good impact parameter resolution provided by the ITS (Fig. 7 left) allows to further exploit the physics capabilities with electrons. As shown in the right panel of Fig. 7, the d_0 distribution of electrons from heavy mesons decay exhibits a significant large tail because heavy mesons have a larger life-time than other particle species. This suggests that by imposing cuts on d_0 one can reduce the combinatorial background and therefore improve the signal-to-background ratio for all sources originating from the primary vertex. Furthermore, the deconvolution of the d_0 distributions allows to estimate the inclusive yield of open charm and open bottom.

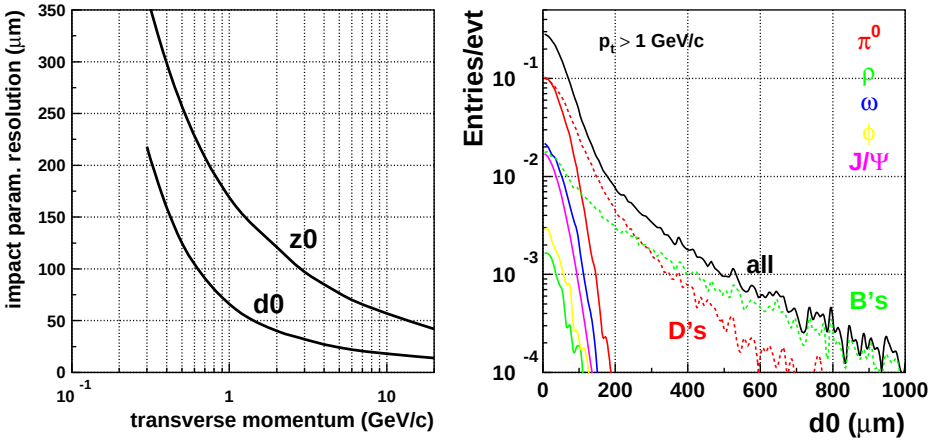

Fig. 7. Left: transverse momentum dependence of the bending (d_0) and the non-bending (z_0) projection of the impact parameter resolution. Right: d_0 distribution of electrons originating from different parent particles.

This is a particularly important measurement for the normalization of the quarkonia signals. It gives also access to the primary p_t of D and B mesons via

[3]The pion multiplicity is so large that, in this case, the number of mis-identified pions is even larger than the number of real electrons in the electron sample identified with the TPC.

the correlation between the p_t of the electron and that of its parent (Fig. 8 left). In addition, it allows to identify secondarily produced J/ψ from B meson decay ($B \rightarrow J/\psi + X$, Fig. 8 right). This is of crucial importance for distinguishing the prompt J/ψ (which are potentially QGP suppressed/enhanced) from the secondary contribution (which should not be directly affected by the QGP). This is even more relevant for the p_t dependence of the J/ψ yield since J/ψ from B meson decay exhibit a much harder p_t spectrum than that of primary J/ψ [26]. As already mentioned, the measurement of secondary J/ψ gives also a direct measurement of the B mesons yield.

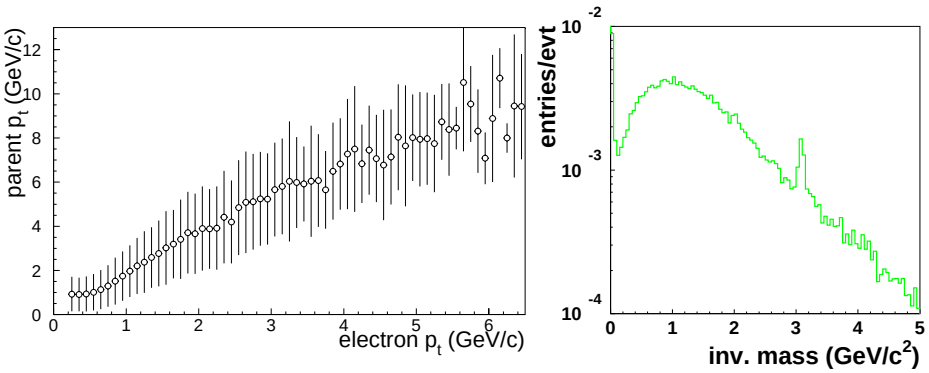

Fig. 8. Left: p_t of the decay electron as a function of the p_t of the heavy meson parent. The vertical error bars correspond to the rms width of the distribution. Right: invariant mass distribution of e^+e^- pairs with displaced vertices.

The expected number of reconstructed Υ per year by ALICE and CMS in minimum bias PbPb reactions is shown in Tab. 2 together with the significance and the Υ detection efficiency.

	ALICE e^+e^-	ALICE $\mu^+\mu^-$	CMS $\mu^+\mu^-$
$\epsilon^{\Upsilon}_{\rm det}$ (%)	1	3.24	5.2
$N^{\Upsilon}_{\rm tape}$	2600	8400	13500
$S/\sqrt{S+B}$ $\Upsilon : \Upsilon' : \Upsilon''$	—	71:36:23	80:32:17

Table 2. Υ detection efficiency, total statistics per year and significance for ALICE in the dielectron and dimuon channels and for CMS in the dimuon channel. The numbers correspond to minimum bias PbPb reactions. $N^{\Upsilon}_{\rm tape}$ includes Υ, Υ' and Υ''. The CMS numbers are from [30]. For more details see the appendix.

The statistics collected by CMS is larger by $\sim 60\%$ than that of ALICE in the dimuon channel. This is essentially due to the larger acceptance of CMS. However, because of the better S/B ratio the significance is comparable or even better for Υ' and Υ'' in ALICE. It is important to stress that the numbers in Tab. 2 were derived according to the largest charged particle multiplicity foreseen. The statistics for ALICE in the dielectron channel is expected to be significantly larger for a collision scenario with a lower charged particle density [27].

4 Hadrons

In the central part of ALICE, heavy mesons and baryons can be fully reconstructed from the measurements of their charged particle decay products in the ITS, TPC and TOF. The most promising decay channel for open charm detection is the $D^0 \rightarrow K^-\pi^+$ decay (and charge conjugate), which has a branching ratio of about 3.9% and $c\tau = 124$ μm. Using the lowest estimate for the charm production rate, one expects 0.55 D^0 (or $\bar{D}^0$) per central PbPb event where D^0 (or $\bar{D}^0$) decays into $K^-\pi^+$ (or the charge conjugate channel) in the acceptance of the central detectors. The strategy for the reconstruction of D^0 mesons includes a number of cuts on various quantities (see [19, 31] for details). The most stringent cuts are that on i) the product of the kaon and pion impact parameters and ii) the pointing angle Θ_p which is the angle between the momentum vector of the D^0 candidate and the line connecting the primary vertex to the candidate decay vertex (Fig. 9).

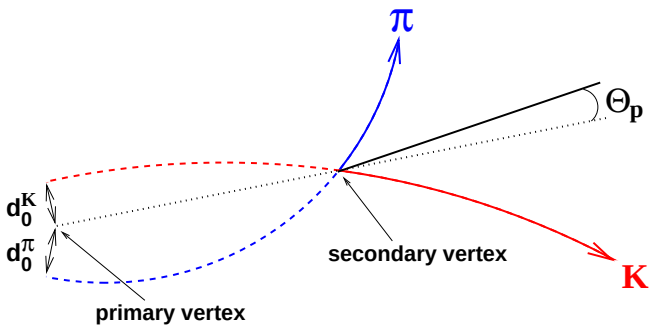

Fig. 9. Schematic representation of the $D^0 \rightarrow K\pi$ decay showing the impact parameters of the kaon (d_0^K) and of the pion (d_0^π) and the pointing angle (Θ_p).

A typical example of invariant mass distribution for D^0 candidates in central PbPb reactions is shown in the left panel of Fig. 10 before and after background subtraction.

The expected statistics is of about 8000 reconstructed D^0 per 10^7 central PbPb events. The corresponding signal-to-background ratio and significance are shown in Tab. 3. Assuming the largest charged particle multiplicity foreseen, the significance if better than 10. This is further improved when the charged particle multiplicity decreases. Note that the numbers in Tab. 3 for $[dN_{ch}/d\eta]_{\eta=0} = 4000$ and 2000 correspond to lower limits based only on a scaling of the number of background pairs with the total multiplicity.

As illustrated in the right panel of Fig. 10, not only the total yield can be measured but also the D^0 p_t distribution. The differential significance is expected to be better than 10 for p_t larger than ~ 1.5 GeV/c.

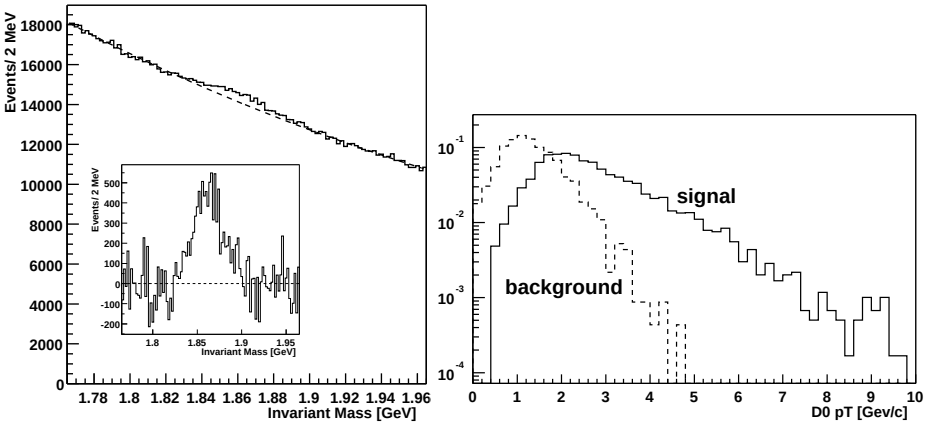

Fig. 10. Left: $K\pi$ invariant mass distribution for 10^7 central PbPb events. Signal and background correspond to the solid and the dashed histograms respectively. The background subtracted distribution is shown in the inset. Right: transverse momentum distribution of D^0 candidates. Signal (solid histogram) and background (dashed histogram) are normalized to the same integral.

$[\mathrm{dN_{ch}}/\mathrm{d}\eta]_{\eta=0}$	8000	4000	2000
S/B (%)	5.3	> 21	> 85
$S/\sqrt{B}$	10.9	> 22	> 44

Table 3. Signal-to-background and significance for reconstructed D^0 mesons assuming a total number of events of 10^7 and various charged particle multiplicities. The numbers correspond to a situation for which at least the kaon is identified. For more details, see [14, 31].

5 Electron-muon coincidences

Heavy mesons decay into e+X or μ+X with a branching ratio of $\sim$ 12% for charm and $\sim$ 10% for bottom. Therefore the correlated $\mathrm{c\bar{c}}$ and $\mathrm{b\bar{b}}$ cross-sections can be measured in ALICE from unlike-sign electron-muon pairs where the electron is identified in the central part and the muon is detected in the forward muon spectrometer. Note that the eμ channel is the only leptonic channel which gives a direct access to the correlated component of the $\mathrm{c\bar{c}}$ and $\mathrm{b\bar{b}}$ pairs. Indeed, in contrast to $\mathrm{e^+e^-}$ and $\mu^+\mu^-$ channels, neither a resonance, nor direct dilepton production, nor thermal production can produce correlated eμ pairs. Within ALICE, the eμ channel has the additional advantage that the rapidity distribution of the corresponding signal extends from $\sim$ 1 to $\sim$ 3, therefore bridging the acceptances of the central and the forward parts of the detector [32]. Measurements of eμ coincidences have already been successfully performed in pp reactions at $\sqrt{\mathrm{s}} = 60$ GeV [33] and in p-nucleon reactions at $\sqrt{\mathrm{s}} = 29$ GeV [34]. They are planned to be done in heavy ion collisions with the PHENIX detector at RHIC [35]. Preliminary simulations have shown the possibility to perform

such measurements with ALICE [21, 26].

6 Summary

ALICE has a broad physics program and excellent capabilities for quarkonia physics. The multitude of envisaged channels discussed are listed in Tab. 4. In addition, further exciting possibilities should be opened with, for example, the reconstruction of B mesons in the hadronic channel and dilepton measurements at very high invariant mass.

probe	channel	acceptance
$J/\psi, \psi', \Upsilon, \Upsilon', \Upsilon''$	e^+e^-	$\|\eta\| < 0.9$
$J/\psi, \psi', \Upsilon, \Upsilon', \Upsilon''$	$\mu^+\mu^-$	$2.5 < \eta < 4$
$c\bar{c}$ & $b\bar{b}$	e^+e^-	$\|\eta\| < 0.9$
$c\bar{c}$ & $b\bar{b}$	$\mu^+\mu^-$	$2.5 < \eta < 4$
D mesons	π,K	$\|\eta\| < 0.9$
B mesons	$B \to J/\psi \to e^+e^-$	$\|\eta\| < 0.9$
D & B mesons	single $e^{\pm}$	$\|\eta\| < 0.9$
$c\bar{c}$ & $b\bar{b}$	$e^{\pm}\mu^{\mp}$	$1 < y < 3$

Table 4. ALICE heavy quarks shopping list.

Appendix: number of reconstructed Υ per year by ALICE and CMS in minimum bias PbPb reactions

The number of reconstructed Υ per year in minimum bias PbPb reactions (N^{Υ}_{tape} in Tab. 2) is estimated according to:

$$N^{\Upsilon}_{tape} = N^{PbPb}_{year} \cdot N^{\Upsilon \to l^+l^-}_{PbPb} \cdot \epsilon^{\Upsilon}_{det}$$

- N^{PbPb}_{year} is the total number of minimum bias PbPb reactions per year:

$$N^{PbPb}_{year} = L \cdot T \cdot \sigma^{PbPb}_{mb} = 4 \cdot 10^9$$

  assuming $L = 5 \cdot 10^{26}$ cm^{-2}s^{-1}, T $= 1 \cdot 10^6$ s and $\sigma^{PbPb}_{mb} = 8$ b;

- $N^{\Upsilon \to l^+l^-}_{PbPb}$ is the number of Υ (Υ+Υ'+Υ'') decaying into $\mu^+\mu^-$ per minimum bias PbPb event:

$$N^{\Upsilon \to l^+l^-}_{PbPb} = [Br \cdot d\sigma/dy]^{pp}_{y=0} \cdot 208^2/2 \cdot 1/\sigma^{PbPb}_{mb} \cdot \Delta y = 6.5 \cdot 10^{-5}$$

  with $[Br \cdot d\sigma/dy]^{pp}_{y=0} = 3 \cdot 10^{-3}$ pb [36], $208^2/2$ is the extrapolation from

pp to minimum bias PbPb assuming a reduction of the cross-section by a factor two to account for nuclear shadowing of the structure functions, $\sigma_{\rm mb}^{\rm PbPb} = 8$ b and $\Delta y = 8$ [36];

- $\epsilon_{\rm det}^{\Upsilon}$ is the Υ detection efficiency (including acceptance, trigger and reconstruction efficiencies).

References

1. J. Schukraft: proceedings of Quark Matter'01, Nucl. Phys. A **698** (2002)
2. T. Matsui, H. Satz: Phys. Lett. B **178** (1986) 416
3. M.C. Abreu et al. (NA50 collaboration): Phys. Lett. B **477** (2000) 28
4. H. Satz: Rep. Prog. Phys. **63** (2000) 1511
5. R. Vogt: Phys. Rep. **310** (1999) 197
6. J.F. Gunion, R. Vogt: Nucl. Phys. B **492** (1997) 301
7. P. Crochet, P. Braun-Munzinger: Nucl. Instrum. and Methods A, in press, nucl-ex/0106008
8. D.E. Groom et al.: Eur. Phys. Jour. C **15** (2000) 1
9. C.M. Ko et al.: Phys. Lett. B **444** (1998) 237
10. P. Braun-Munzinger, K. Redlich: Eur. Phys. J. **C 16** (2000) 519
11. P. Braun-Munzinger, J. Stachel: Phys. Lett. B **490** (2000) 196
12. R.L. Thews, M. Schroedter, J. Rafelski: Phys. Rev. C **63** (2001) 054905
13. M.I. Gorenstein, A.P. Kostyuk, H. Stoecker, W. Greiner: Phys. Lett. B **509** (2001) 277
14. ALICE collaboration: Physics Performance Report, in preparation
15. R. Baier, D. Schiff, B.G. Zakharov: Ann. Rev. Nucl. Part. Sci. **50** (2000) 37
16. P. Giubellino for the ALICE collaboration: these proceedings
17. Y. Foka for the ALICE collaboration: these proceedings
18. J.P. Revol: these proceedings
19. ALICE collaboration: ALICE Technical Proposal, CERN/LHCC **95-71** (1995)
20. ALICE collaboration: MUON Spectrometer Technical Proposal, CERN/LHCC **96-32** (1996)
21. ALICE collaboration: TDR of the MUON Spectrometer, CERN/LHCC **99-22** (1999)
22. ALICE collaboration: Addendum 1 to the TDR of the MUON Spectrometer, CERN/LHCC **2000-046** (2000)
23. A. Morsch for the ALICE collaboration: Nucl. Phys. A **638** (1998) 571c
24. http://AliSoft.cern.ch/offline/
25. A. Morsch: private communication
26. ALICE collaboration: TRD Technical Proposal, CERN/LHCC **99-13** (1999)
27. ALICE collaboration: TDR of the TRD, CERN/LHCC **2001-021** (2001)
28. A. Andronic et al.: IEEE Trans. Nucl. Sci. **48** (2001) 1259
29. K. Gallmeister, B. Kaempfer, O.P. Pavlenko: Eur. Phys. J. C **8** (1999) 473
30. M. Bedjidian, private communication
31. A. Dainese, R. Turrisi, N. Carrer: ALICE internal note, in preparation
32. Z. Lin, R. Vogt: Nucl. Phys. B **544** (1999) 339
33. A. Chilingarov et al.: Phys. Lett. B **83** (1979) 136
34. T. Akesson et al. (HELIOS collaboration): Z. Phys. C **72** (1996) 429
35. PHENIX collaboration: Conceptual Design Report, BNL **48922** (1993)
36. R. Gavai et al.: Int. J. Mod. Phys. A **10** (1995) 3043